

Title

Experimental and numerical study of the influence of the plenum box on the airflow pattern generated by a swirl air diffuser.

Abstract

When CFD is employed to design a ventilation system, one of the most delicate aspects is the modeling of the diffuser. The designer has different choices, which range from simulating the detailed geometry of the diffuser, including the plenum box, to use special boundary conditions to reproduce the velocity profile in each slot of the diffuser. This study is carried out to examine the influence of the plenum box on the turbulent airflow pattern generated by a swirl air diffuser from the experimental and numerical points of view. First, we perform experiments to evaluate such influence. Then, these experiments are contrasted with two numerical approximations to the problem using the Fluent 6.3.26 commercial CFD software. We first perform a simulation of the complete diffuser geometry -including the plenum box- and later a simplified simulation of the diffuser, where the whole geometry is simplified to a plane in which the velocity components and the slots positioning are specified via a particular boundary condition. The main findings of this study reveal that the simplified simulation is good enough at close range, while in the remote flow field the differences between both approaches practically disappear.

Nomenclature

C_2	pressure-jump coefficient, m^{-1} .
C_d	discharge coefficient
D_h	Hydraulic diameter, m
n	number of slots
Q	diffuser airflow rate, m^3/s
q	slot airflow rate, m^3/s
R	Radial coordinate, m
Re	Reynolds number
v	air velocity, m/s
v_x, v_y, v_z	air velocity components, m/s
x, y, z	coordinates
y^+	distance normal to surface in wall units
α	screen permeability, m^2 .
ρ	air density, Kg/m^3
μ	dynamic air viscosity, Pa·s
ϕ_v	volumetric dissipation of mechanical power, W/m^3
Δ_p	pressure drop, Pa
Δ_m	porous medium thickness, m.

1. Introduction

At the present moment the use of Computational Fluids Dynamics (CFD) techniques in the design of ventilation systems in rooms is widespread [1]. Correctly validated CFD models provide detailed information on the flow field in rooms, whilst permitting an assessment of ventilation efficiency.

An accurate simulation of the airflow pattern in a room with a particular ventilation strategy depends deeply on the boundary conditions, especially the air supply openings. Consequently, it is necessary to properly incorporate these elements into the CFD simulations so as to give an accurate prediction of the flow field [2,3]. The geometric conditions of modern-day air diffusers are as a rule complex, and therefore difficult to reproduce in detail in computational models [4,5]. Different methodologies are employed in CFD to model diffuser boundary conditions: simplified geometry, box-method, prescribed velocity, momentum methods and a method where the detailed diffuser geometry is included in the computational domain [6–8].

Simplified models have been widely used to represent different types of diffusers. Koskela et al. [9] highlight the difficulty of correctly representing the diffuser by means of a simplified model to achieve a suitable relationship between air velocity, momentum and the effective area of the diffuser. The effective air outflow area is less than the free area, and although the condition of continuity is met the diffuser does not introduce the same amount of momentum as in authentic conditions.

Another option is to replace the diffuser with a more detailed boundary condition. Heikkinen [10] achieves good approximation by replacing the diffuser with several slots, the total area of which coincides with the effective area of the diffuser. However, Chen and Moser [11] conclude that this method does not produce good results in non-isothermal simulations. Nielsen [12] develops the box method, whereby the region adjacent to the diffuser is replaced by an imaginary box onto the surface of which the velocity boundary conditions are imposed; thus the problem of the effective area is eradicated and fine meshing of the diffuser zone is not required [13]. The momentum method separates the boundary conditions for continuity and momentum. It makes it possible to resolve the difference between the effective and free areas. Mohammed et al. [14] replace the diffuser with a set of N points on its periphery, in this way reproducing the main features of the outflow. They suggest it is a simple method that could be implemented in commercial software and one which reduces computation times. In the study of Zhang et al. [6] there is a review of the most commonly used methods.

Nielsen [1] indicates that a simple and trustworthy method is still being sought for the majority of diffusers. Several authors [15–17] show that these methods rigorously approximate to diffuser behaviour, although one of them requires experimentation which is not always possible.

Swirling diffusers are commonly used in the service sector and they are designed to create a flow field with a high degree of mixing [5,18–20]. The diffusers are usually connected to the ventilation duct by a plenum box [16] or sometimes directly connected to the duct [14,21]. Most assemblies involve diffusers attached to a plenum box, although the latter tends not to be taken into consideration when CFD simulations are carried out.

In this study a diffuser is considered to be comprised of two elements: the plenum box and the diffuser front. The airflow pattern in the region close to the diffuser front is influenced by both

elements. Despite the fact that the plenum box causes differences in the close-range airflow pattern, it is worth analysing how such differences affect the flow field downstream of the diffuser front. An evaluation of the velocity field close to a swirl diffuser has been conducted with a 3D ultrasonic anemometer for two plenum boxes: one with a side inlet and screen to equalise flow inside the box, and a second with a vertical inlet and no screen. We assess how the type of plenum box modifies the velocity field near to the diffuser outlet. These measures are employed to validate a CFD model which represents the geometry of the whole diffuser. The CFD model allows a better understanding of flow behaviour inside the plenum box. Finally, we analyse the sensitivity of the in-room airflow pattern to the methodology used so as to represent the diffuser with a boundary condition.

The final aim of this research is to replace the entire geometry of the swirl diffuser with an equivalent simplified boundary condition. Lastly, an assessment is made of the attenuated impact of the plenum box on the airflow pattern in the room the greater the distance from the diffuser.



a)



b)

Fig. 1. a) Diffuser in the experimental setup. b) Swirling vanes in the diffuser front

2. Experimental study

An experimental study is made of the spatial development of the airflow pattern generated by a Kool-Air DF-RO-24 swirl diffuser front. This diffuser comprises a square diffuser front with 24 slots, Fig. 1. Each slot has a swirling vane on the inside, Fig. 1b. Discharge directions can be altered by adjustment of the vane angle. For this study, the swirling vanes are set to 45° and oriented so as to create an external swirl. Table 1 shows the most important characteristics of the diffuser.

Table 1. Diffuser characteristics

Airflow rate	604 m ³ /h
Plenum box inlet diameter	0.25 m
Reynolds number based on plenum box inlet	5.7×10^4
Diffuser dimension	$0.6 \times 0.6 \times 0.35$ m ³
Diffuser outlet area	0.074 m ²
Number of slots	24
Slot angle	30°
Slot dimensions	154 × 20 mm ²
Reynolds number based on the slot, D_h	7.6×10^3
Guide vane angle	45°
Guide vane width	29.6 mm

The removable diffuser front is held in the plenum box with a central screw. Air is supplied via side entry, plenum box A, Fig. 2a, or top entry, plenum box B, Fig. 2b. When air is supplied laterally to the plenum box there is a perforate steel plate to ensure an equal air distribution. When air is supplied via top entry there is no internal element in the plenum box. In all other respects both plenum boxes are the same.

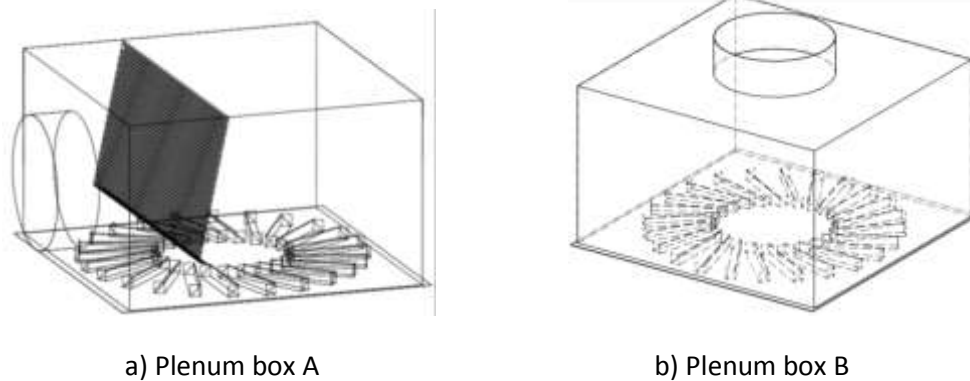


Fig. 2. Outline of the diffusers

The quasi-radial positioning of the diffuser front slots implies that the lower the radial coordinate the closer the slots are to each other. This causes greater interaction between slot jets near the centre than those on the periphery.

2.1. Experimental setup

The experimental installation reproduces a suspended ceiling in a room in which a swirl diffuser is placed in the centre, Fig. 1. An outline of this is displayed in Fig. 3. The installation is that of a space 3×3 m² and 2.5 m high. The four walls do not reach the floor, with the result that air from the diffuser leaves the space at the sides at floor level. The diffuser is placed in the centre of the ceiling far enough away from the walls to prevent them from having an influence on the airflow near the diffuser. The aim of the walls is to avoid disruption during measurement from external air currents to the diffuser airflow.

Air is supplied by a fan equipped with a frequency inverter which makes it possible to control the flow rate. The fan is attached to a duct on which there is an orifice plate, with a 2% uncertainty flowrate

measurement. The last section before the plenum box is straight and its length is ten times the diameter of the duct. Air leaves the plenum box via the diffuser front slots.

The anemometer is placed at the end of a 3D traverse system, which in turn is set on a manually operated system of rails permitting horizontal movement. The displacement system does not cause alteration to the flow in the measurement area. The traverse system has excellent repeatability and a 0.02 mm positioning uncertainty. However, due to the system of rails the final positioning uncertainty of the anemometer is 1 mm in the three directions.

The velocity of air is measured with a Kaijo WA-590 ultrasonic anemometer [9,17,22]. This simultaneously evaluates the three components of the velocity at a range of 0 m/s to 10 m/s, with 2% uncertainty, 0.005 m/s resolution and 10 Hz sampling frequency. The anemometer is composed of three pairs of ultrasonic sender-receivers. The distance between each transmitter and receiver is 5 cm, therefore the velocity provided by the anemometer is the average velocity in a volume of measurement of $5 \times 5 \times 5 \text{ cm}^3$. A specific software runs both the movement of the traverse system and data collection.

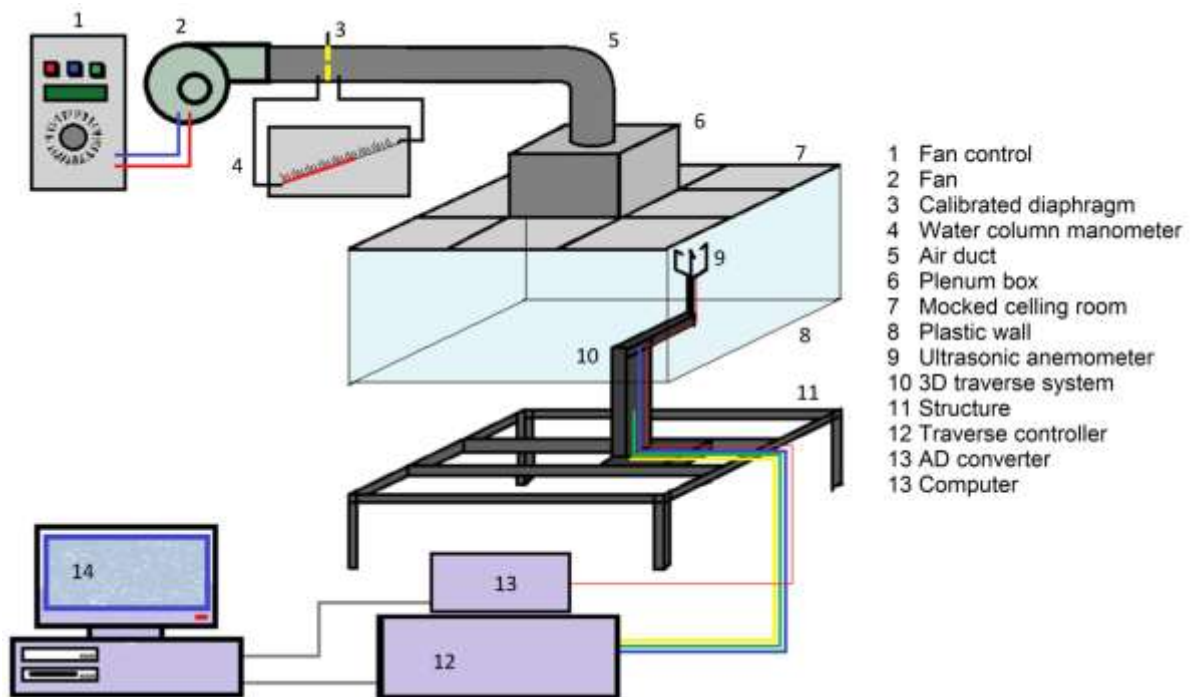


Fig. 3. Outline of the experimental installation

The origin of the coordinates is in the centre of the diffuser. The X and Y axes are horizontal and the Z axis vertical and towards the floor. In the plenum box with a side inlet the Y axis is situated towards the air inlet. Measurements are taken on three horizontal planes at $z = 53 \text{ mm}$, $z = 106 \text{ mm}$ and $z = 159 \text{ mm}$. On each horizontal plane measurements are taken from $x_{\min} = -60 \text{ cm}$ to $x_{\max} = 60 \text{ cm}$ every 5 cm and from $y_{\min} = -60 \text{ cm}$ up to $y_{\max} = 60 \text{ cm}$ every 5 cm, that is, 625 positions on each one.

The averaging time required depends on the duration of the fluctuation periods. The influence of the averaging time on measurements has been ascertained by means of 20-minute sampling at a frequency of 10 Hz at different locations. A mean of 20 minutes is taken as a reference value for the average velocities. Deviation from this reference depending on the averaging time is shown in Fig.

4. For the sake of clarity, only averaging periods of less than 2 minutes are represented. For averaging times above 1 minute deviation is lower than 2%, as a result of which 1 minute is established as the measuring time. More than 12 hours are required to measure a horizontal plane. Four sessions of slightly over 3 hours each are necessary. On the $x=0$ and $y=0$ lines measurements are duplicated but conducted at different times, with a time lapse of at least three hours. These duplicated readings have been employed to check the repeatability of the tests.

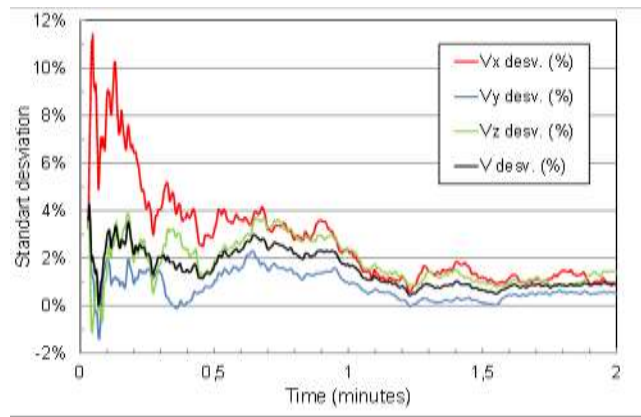


Fig. 4. Deviation of the instant air velocity as against the reference values with a 20-minute averaging time

2.2. Experimental results

The rectangular jet produced in each of the 24 slots is diverted to the ceiling as a result of the Coanda effect. This airflow develops radially and parallel to the ceiling. The Coanda effect is clearly appreciated in Fig. 5. The streamlines run close to the ceiling as the airflow progresses radially. It can also be observed how these lines ascend in the centre due to the suction effect and how, when developing radially towards the edge of the diffuser, they go rapidly towards the ceiling. The streamlines have been obtained by using only the velocity components on the plane.

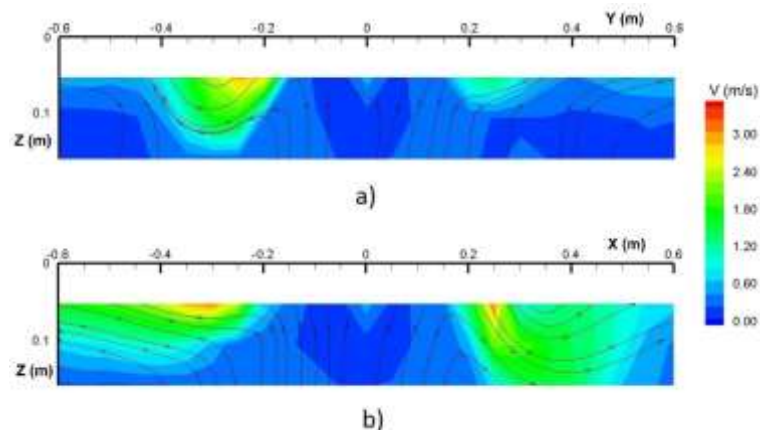


Fig. 5. Distribution of the velocity magnitude for diffuser A. a) plane $x=0$, b) plane $y=0$

Fig. 6 represents the contours of the velocity module and the streamlines (calculated with v_x and v_y) on the $z=53$ mm plane, parallel to the diffuser front. The lines show that the airflow pattern generated by the diffuser is in essence radial with a rotational (tangential) component.

There is an area of low velocities around 0.2 m/s in the centre of the plane (in blue). It can also be seen that there is a region in the shape of a circular crown with high velocities (in red) at approximately 25 cm from the centre of the diffuser.

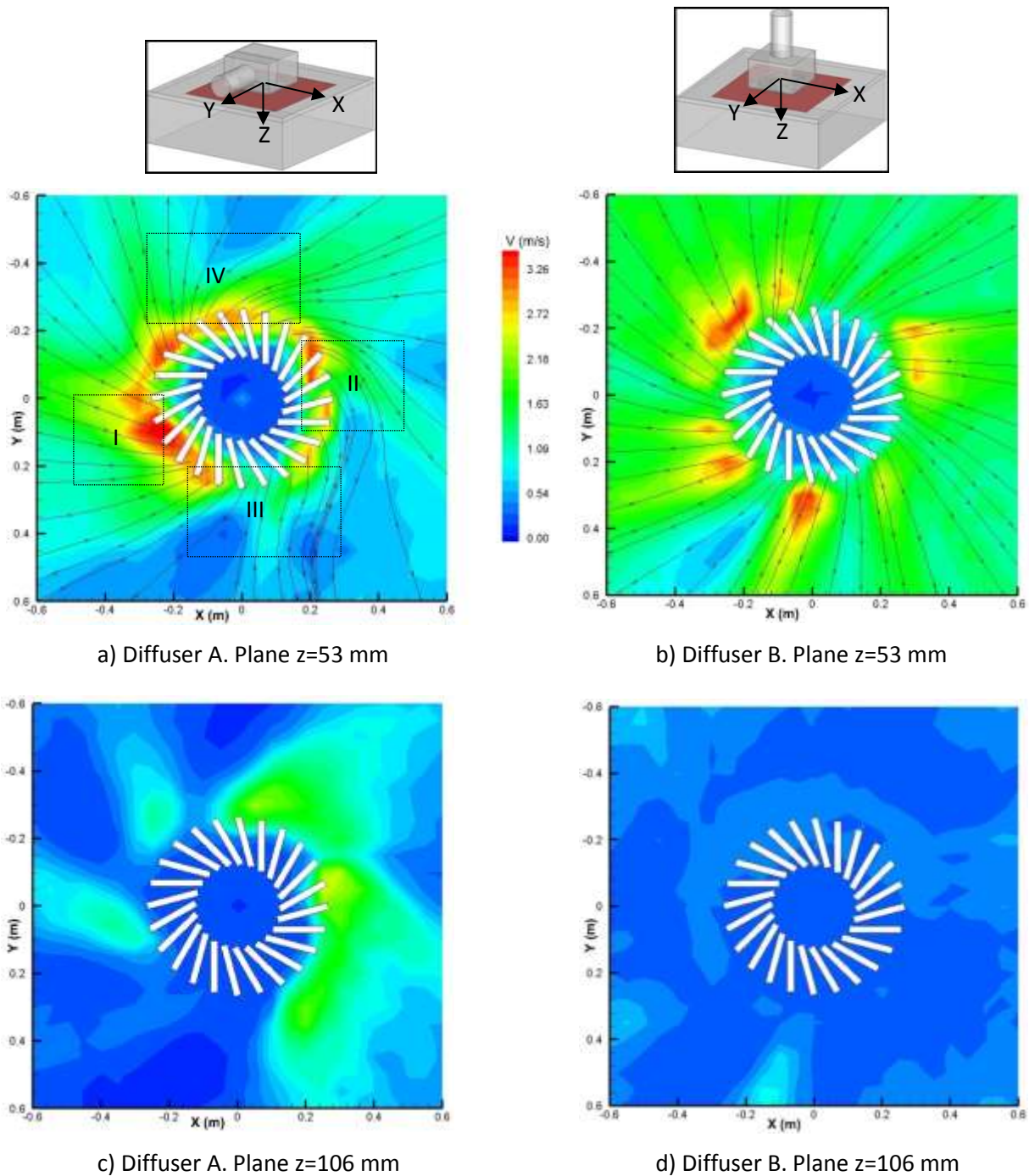


Fig. 6. Distribution of the velocity magnitude on horizontal planes. Diffuser A (left), diffuser B (right) plane z=53 mm (up), plane z=106 mm (down)

The general tendency of the air leaving the diffuser, Fig. 6, is to follow a tangential flow pattern induced by the relative position between the slots and the inclination of the vanes. The air flow pattern in diffuser B is fairly symmetrical, which is not the case for diffuser A. In the latter the air input is lateral, causing an asymmetrical outflow pattern. Interpreting the airflow inside the plenum box is difficult due to the large number of factors involved and its complex geometry. However, it

obviously has an effect on the flow field close to the diffuser front. The experimental results do not permit a profound evaluation.

Four clearly identifiable regions are established to analyse the lack of outflow symmetry for diffuser A, Fig. 6a. In zone I velocity is greater than elsewhere since the vanes, set in front of the slot, are in the direction of the air inflow. This results in better guidance and a more intense Coanda effect, Fig. 5. In zone II the opposite occurs, the velocity being lower (Fig. 6a) and the air is not so bent to the wall, Fig. 5. Zone III corresponds to the air intake area in the plenum box. Zone IV behind the screen is not significantly sensitive to this alignment with the air inlet.

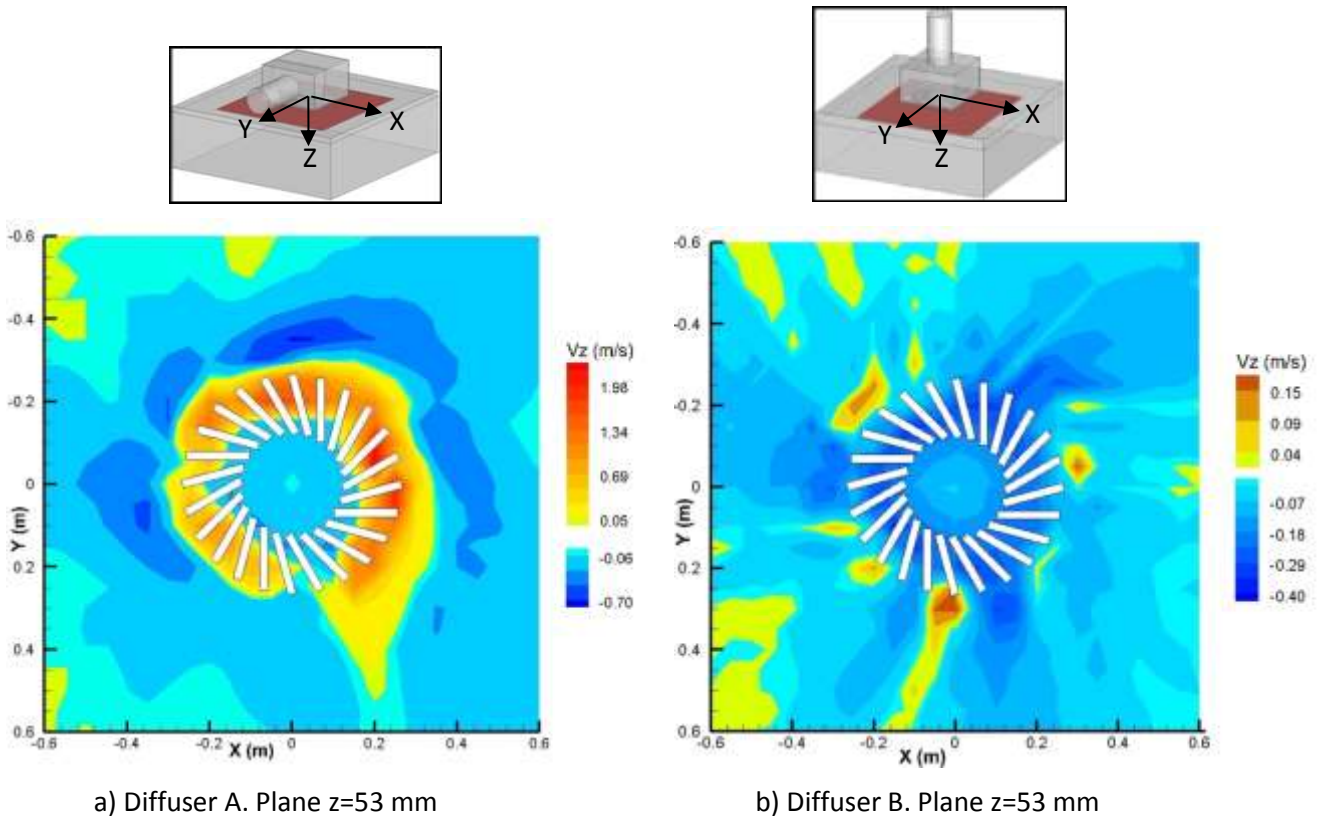


Fig. 7. Distribution of v_z on horizontal planes $z=53$ mm. A) diffuser A, b) diffuser B.

As the distance to the diffuser front increases the velocity diminishes to a greater extent for diffuser B than for diffuser A, Fig. 6. This happens because with diffuser B the Coanda effect is more noticeable, the airflow adheres more to the ceiling and the velocity on $z=106$ mm is very low. Consequently, it is difficult to measure on planes which are further from the ceiling. The same can be deduced if an analysis is made on the $z=53$ mm plane of v_z (Fig. 7a and Fig. 7b). In the case of diffuser B, the flow from the diffuser causes the entire airflow to rise. In diffuser A, as the Coanda effect is less strong, there is still some descending airflow coming from the diffuser. The suction effect is witnessed in the central area around the diffuser front axis, where the streamlines are rising, Fig. 5.

It can be concluded from measurement of the velocity field that on parallel planes near the diffuser front, even if the geometry of the latter is periodic, the airflow pattern at the outlet is not symmetrical if the flow in the plenum box is not symmetrical. In addition, it has been seen that on planes which are at a sufficient distance the flow pattern is similar for both diffusers.

3. Numerical model

The present study employs the RNG k-ε turbulence model [23] along with the Navier-Stokes equations for the turbulent airflow modeling using the commercial software Fluent v6.3.26. This choice is based on the strength of its performance in predicting different types of ventilation flows [24] and because of its accuracy for rapidly strained flows, including the effect of swirl. The equations of the model are listed in [25].

Regarding the discretization, second order schemes are used for all flow variables and the pressure velocity coupling algorithm used is the SIMPLE scheme from Patankar [26]. To model the flow near walls, standard wall functions are used, always ensuring y^+ values above 30 and below 100 for all the simulation runs. The calculations are considered to have converged when the estimated residuals are stable at around 10^{-5} .

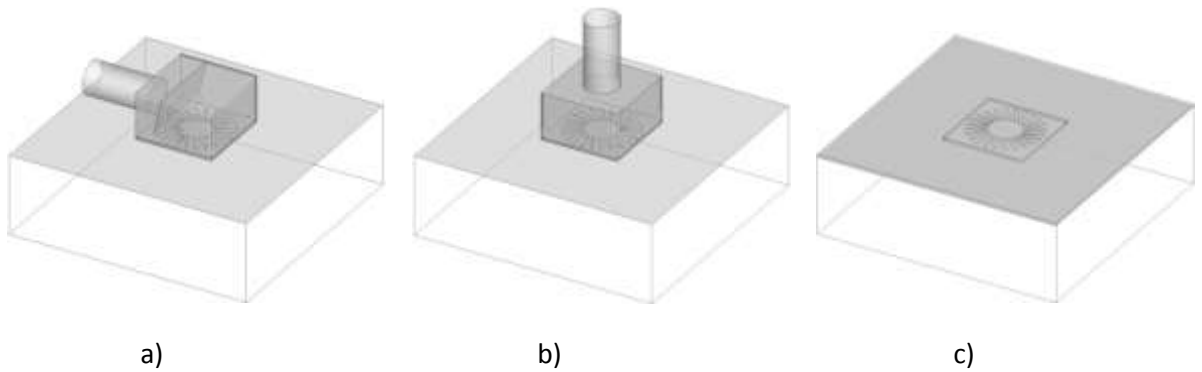


Fig. 8. Computational domains.

Three geometric models of the diffuser have been made: geometry A with a side-entry plenum box, Fig. 8a; geometry B with vertical entry, Fig. 8b; and a geometry C without a plenum box, Fig. 8c. For geometries with a plenum box an admission duct length, equal to twice its diameter, is included.

Hybrid meshes, results of a combination of hexahedra and tetrahedra are used. The mesh is refined close to slots and vanes, and in the screen of the plenum box A. The diffuser front is also refined to reproduce the complex flow pattern there. A grid sensitivity study is carried out using different meshes with increasing number of cells, reaching grid independence for geometries A and B with grids around 500k cells and 60k cells for geometry C. It is also remarkable that for plenum box A, the internal perforated plate effect is treated as a porous zone [27], where the pressure change is computed using a combination of Darcy's law and additional inertial loss terms:

$$\Delta_p = - \left(\frac{\mu}{\alpha} v + C_2 \frac{1}{2} \rho v^2 \right) \Delta_m$$

where v is the velocity normal to the screen. In order to determine the coefficients α and C_2 , we have measured the difference of pressure (Δ_p) produced by the screen for several air velocities (v). In Fig. 9, we see the experimental data and the adjustment curve with $\Delta_m=1$ mm, $\alpha=1.27855 \times 10^{-8}$ m² and $C_2=1.3780 \times 10^4$ m⁻¹.

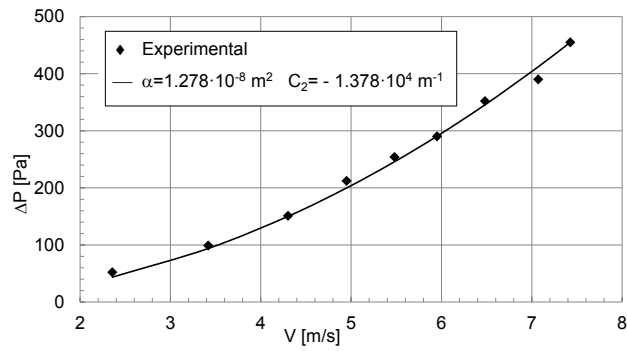


Fig. 9. Pressure drop through the diffuser A screen

In all the simulations involving the plenum box, a uniform flow boundary condition is imposed in the inflow duct. Turbulent boundary conditions are fixed using a turbulent intensity of 10% and the hydraulic diameter of the inflow duct.

3.1. Validation of the model

For validation of the numerical model we have compared the numerical and experimental findings for the most representative planes. It should be pointed out in section 2.1 that the measurements taken with the ultrasonic anemometer was a velocity averaged in the measurement volume. As a result, for a proper comparison it is necessary to average the CFD velocity results in a volume similar to the measurement volume.

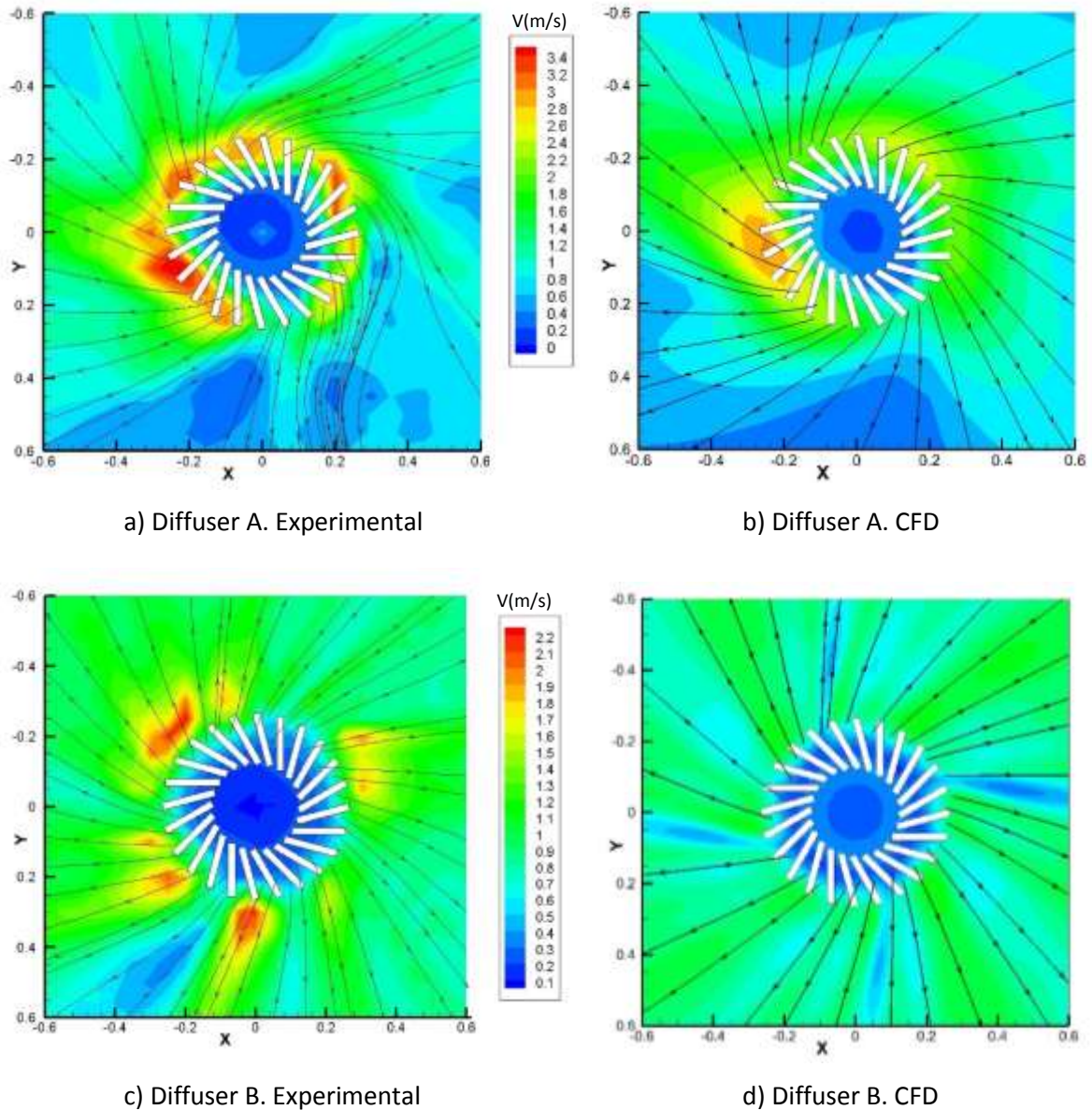


Fig. 10. Velocity magnitude and streamlines. Experimental vs. CFD. Plane $z=53$ mm

Fig. 10 displays a comparison of numerical and experimental results for a plane next to the diffuser front, which is where the airflow field is more complex. The flow pattern is equivalent. In both the numeric and experimental results it may be observed how the tangential velocity component in diffuser A is greater than that of diffuser B. The streamlines reflect the close similarity of the air direction, although the velocity module has slightly lower numerical results. Perhaps this is because in the numerical simulation the air jets from the slots are adhered to the ceiling to a greater extent, with the result that the velocity diminishes at a faster rate along with distance from the diffuser front.

For a more in detail analysis of the velocity field, we take the averaged field of velocity on a vertical radial plane. The diffuser is not cylindrically symmetrical, unlike, generally speaking, the mean flow field; therefore, we may consider a radial average to represent the close-range flow field.

Let us suppose a vertical plane with one edge on the diffuser axis and the other in a radial direction. In a cylindrically symmetrical airflow field a turn at a certain angle in respect of the axis would produce an identical field. Consequently, the averaging process involves taking the mean between each point of the planes revolving around the diffuser axis. In this way we can obtain a plane representative of the entire volume close to the diffuser.

Fig. 11 shows the averaged module of the velocity field calculated as described above on different radial planes for diffuser A. It is clear that the experimental data is well predicted by the CFD model, especially close to the diffuser outlet (plane $z = 53$ mm). Far away from the diffuser, at plane $z = 106$ mm, the velocity distribution is equivalent, although the prediction is not as good as in the previous case. This case is representative for the whole set of measurements and calculations.

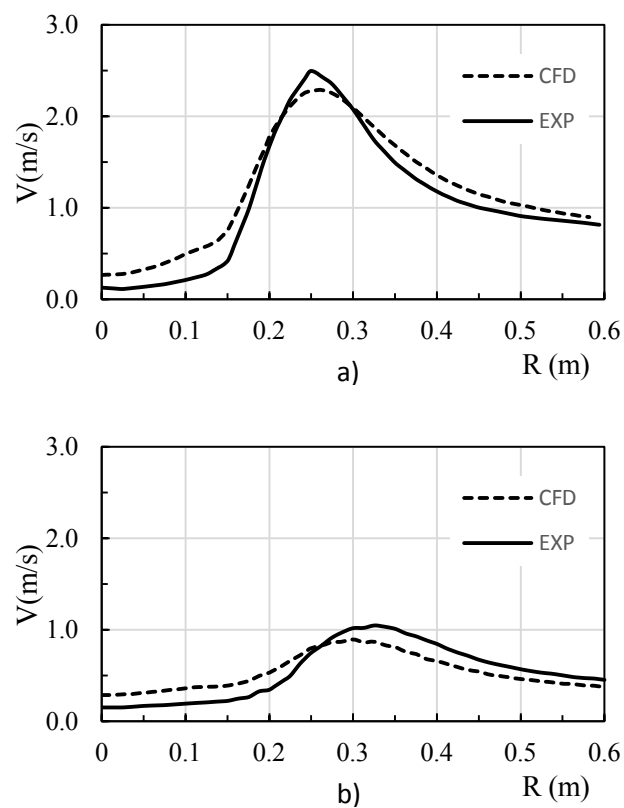


Fig. 11. Averaged module of velocity on a radial plane in diffuser A. Experimental vs. CFD. (a) $z = 53$ mm (b) $z = 106$ mm.

3.2. Numerical results

The numerical results provide us with a detailed knowledge of the airflow inside the plenum box and how this determines the flow pattern at the diffuser outlet. Here we find the same three effects, namely, rotation, adherent flow and suction, which were observed in the measurements.

Fig. 12 demonstrates the magnitude of velocity on a vertical plane containing the duct axis. In diffuser A, at the side inlet of the plenum box there is a stagnation zone on account of the screen, resulting in excess pressure. Part of the airflow goes through it whilst some avoids it and passes underneath. Next, the air is supply through the diffuser slots. The air leaving the diffuser forms a

current that adheres to the ceiling. The entire region below the diffuser is characterised by rising air in the room as a result of the suction effect produced by the current. As may be expected, the plenum box of diffuser B induces a more axisymmetric outflow. In Fig. 12b) it can be observed that the volumetric dissipation of mechanical energy (Φ_v , W/m^3), which accounts for the irreversible transformation of mechanical energy to internal energy, is greater in diffuser A. The screen is responsible for additional losses, the total dissipation being 1.55 times greater in this case, and most of the dissipation can be observed in the region of the vanes.

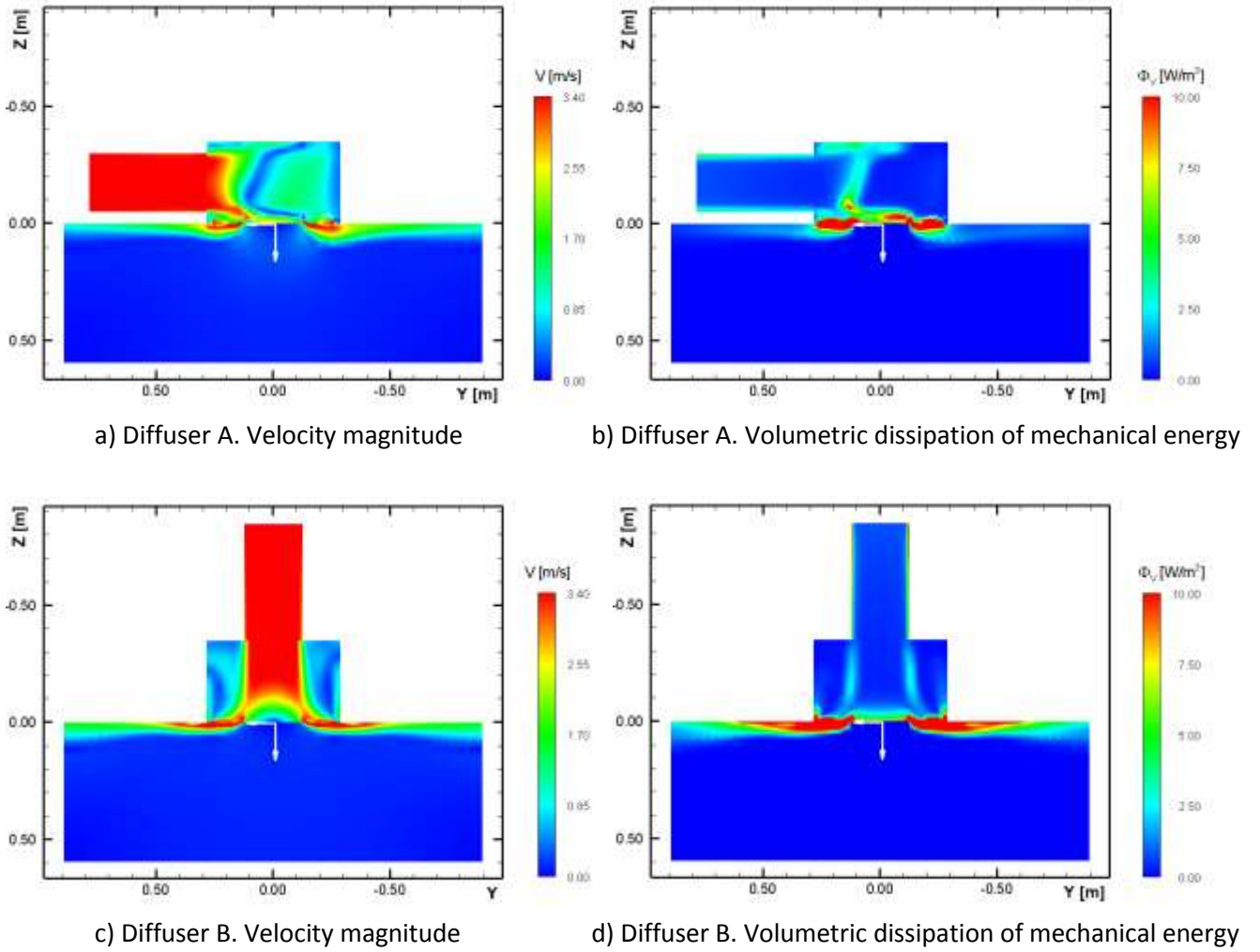


Fig. 12. Distribution of the velocity magnitude and dissipation of mechanical energy. Plane $x=0$ m

The discharge coefficient C_d of each slot on the diffuser front is defined as:

$$C_d = \frac{q}{Q/n} \quad (1)$$

This non-dimensional coefficient depicts how the diffuser flowrate is split among the slots.

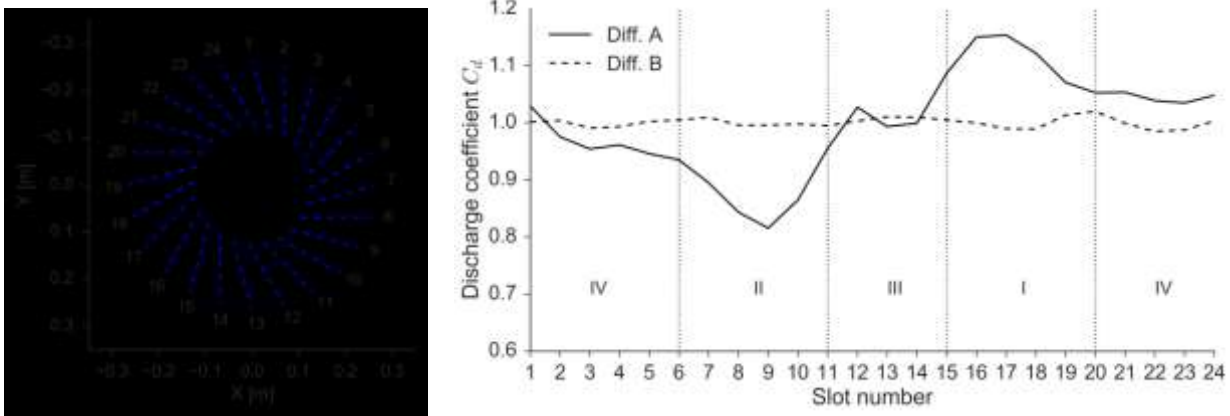


Fig. 13. Discharge coefficient C_d of the diffuser slots

In Fig. 13 we can see the value of this C_d coefficient for the front slots of diffusers A and B. The top air entry of diffuser B makes the plenum box airflow symmetrical, as a result of which the C_d coefficient for all the slots is similar and near to 1. In diffuser A it can be seen that this coefficient is greater than 1 in region I (slots 15 to 19). In region II (slots 6 to 10) this coefficient is minimal. In region III (slots 11 to 14) it is approximately 1. If we analyse the position of the vanes relative to the flow passing under the screen, in region I the inclination is in the same direction, whilst in region II it is the other way; in region III they are aligned and in IV, as it is behind the screen, the influence of the tilt is minimal; however, the vanes next to region I (favourable tilt) have a C_d slightly higher than the ones next to region II (unfavourable tilt).

Fig. 14 shows the ratio between the z -velocity and the mean z -velocity for each slot (in percentage), in a coordinate system fixed to the slot edge closer to the centre of the diffuser front (an increasing slot length implies increasing distance from the centre of the diffuser front).

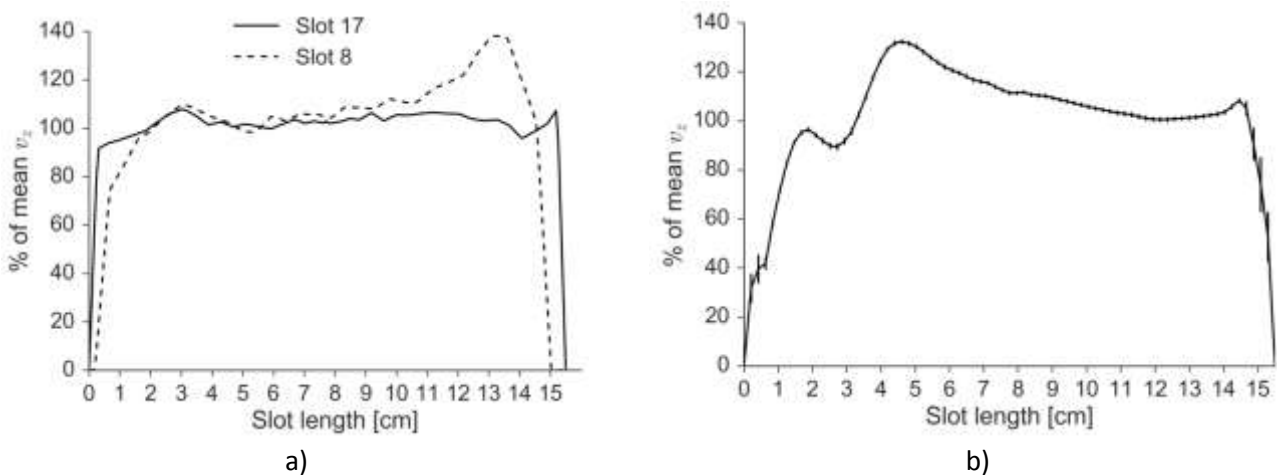


Fig. 14. Distribution of the v_z along the slot. a) Diffuser A (slots 8 and 17) b) Diffuser B. (average and standard deviation for all of slots)

In diffuser B the flow distribution in each slot is similar. The airflow around the centre of the diffuser front is seen to be greater than that of the periphery. This might be the result of two effects. Firstly, part of the inflowing air is found in this area and, what is more, increased interaction

between the slot jets would favour greater suction. In diffuser A, depending on the vane setting, there is a different flow distribution along the slot.

There is a clear influence of the plenum box on the airflow pattern near the diffuser front as well as on energy losses. Nevertheless, in terms of the movement of air in the room, if we observe the velocity fields in Fig. 12, it may be concluded that at a distance from the diffuser the flow field is quite similar and that the differences resulting from the plenum box only show up near the outlet.

3.3. Influence of the methodology

In this section we compare the numerical results obtained with two different methodologies for simulating the diffuser. The first, which has been described previously, has been to provide a complete simulation of the diffuser. In the second, only the diffuser front is simulated. The volume adjacent to the diffuser is the same in both approaches.

When a simulation is made of only the diffuser front, it is supposed that the airflow is perfectly directed by the vanes and, as a result, the air flows uniformly at an angle of 45 degrees out of each of the 24 slots on the diffuser front. Since we do not reproduce either the duct, the plenum box, or the vanes, the mesh consists of only 60,000 cells, a much lower number than that of the other approach. This methodology is completely justifiable for diffuser B, if we consider the results shown in Fig. 13 and Fig. 14. For diffuser A its use should be evaluated.

For an analysis of the differences between methodologies, we take the averaged field of velocity on a vertical radial plane, as explained at the end of Section 3.1, thus considering a radial average to represent the close-range flow field.

Fig. 15 shows the velocity field on the radial plane averaged out for both methodologies. It may be appreciated how the flow pattern is similar in the three cases, and that only in the area which is very close to the diffuser can any difference be seen, particularly for diffuser A. In the less close $Z > 0.15$ m region the differences in the airflow pattern are minimal.

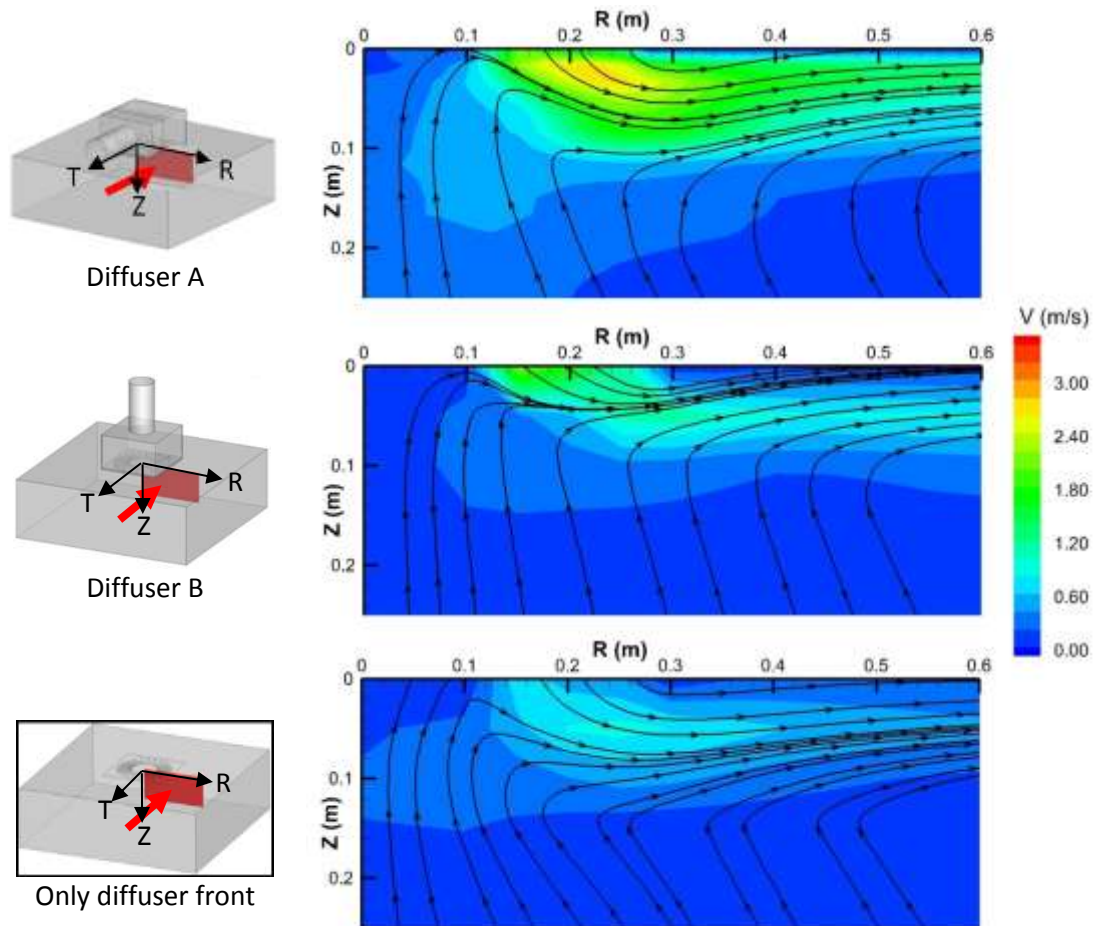


Fig. 15. Averaged module of velocity and streamlines on a radial plane. Diffuser A (top), diffuser B (middle) and only diffuser front (bottom).

These findings reveal that the simplified geometric model is capable of reproducing the airflow field in a room in a similar way to the detailed simulation model. The former, with 90% fewer cells, requires much less calculation time. Moreover, it could be easily implemented in existing models by a slight modification of the meshing. Such characteristics make this option suitable for indoor air simulations.

4. Conclusions

An analysis has been made of the airflow field of two 24-slot rotational diffusers with vanes: one with a plenum box with a side air inlet and the other diffuser with a top inlet. First of all, an experimental evaluation was made, by means of a 3D ultrasonic anemometer, of the flow pattern close to the diffusers and the effect of the plenum box on this pattern was studied. It has been seen that the close-range flow field is characterised by adherence of the slot jets to the ceiling. This adherence is more noticeable in the case of the top inlet diffuser. The flow pattern is highly three-dimensional, axisymmetric for the top inlet diffuser and non-symmetrical for the side inlet diffuser.

A CFD model has been developed to simulate the flow field inside the diffusers and in the room. Validation of the model has been attested to with the experimental results. An analysis was made of the airflow inside the two diffusers and the distribution of slot flow rate was determined. This

distribution was uniform for the top inlet diffuser but not in the case of the side inlet diffuser. It may be established from the results that the top inlet diffuser causes less dissipation of energy and generates a more symmetrical flow field in the adjacent area than the diffuser with the side inlet.

Finally, we have assessed the possibility of simulating the rotational diffuser without its plenum box, establishing the boundary condition directly on the air outflow slots. With the proposed method of simulating the diffuser without the plenum box things can be simplified to a greater extent; besides, the complexity of the meshing and calculation time diminishes. The simulations of the airflow field in the room are appropriate.

5. Acknowledgements

This research was supported by project DPI2014-55357-C2-1-R R from the Spanish National Government 2013-2016 R&D&I plan issued by the Ministry of Economy and Competiveness. This project is cofinanced by the European Regional Development Fund (ERDF).

6. Bibliography

- [1] P. V Nielsen, Fifty years of CFD for room air distribution, *Build. Environ.* 91 (2015) 78–90. doi:10.1016/j.buildenv.2015.02.035.
- [2] T. Yao, Z. Lin, An experimental and numerical study on the effect of air terminal types on the performance of stratum ventilation, *Build. Environ.* 82 (2014) 431–441. doi:10.1016/j.buildenv.2014.09.021.
- [3] D. Etheridge, M. Sandberg, *Building ventilation: theory and measurement*, John Wiley & Sons, Chichester, 1996.
- [4] H.T. Xu, J.L. Niu, A new method of CFD simulation of airflow characteristics of swirling floor diffusers, in: *Eighth Int. IBPSA Conf.*, Eindhoven, Netherlands, 2003.
- [5] B. Sajadi, M.H. Saidi, A. Mohebbian, Numerical investigation of the swirling air diffuser: Parametric study and optimization, *Energy Build.* 43 (2011) 1329–1333. doi:DOI: 10.1016/j.enbuild.2011.01.018.
- [6] T. Zhang, K. Lee, Q. Chen, A simplified approach to describe complex diffusers in displacement ventilation for CFD simulations, *Indoor Air.* 19 (2009) 255–267. doi:10.1111/j.1600-0668.2009.00590.x.
- [7] P. V. Nielsen, Description of supply openings in numerical models for room air distribution, *ASHRE Trans.* 98 (1992) 963–971.
- [8] E. Djunaedy, *Numerical modelling of supply openings for room air distribution*, National University of Singapore, 2000.
- [9] H. Koskela, Momentum source model for CFD-simulation of nozzle duct air diffuser, *REHVA Sci.* 36 (2004) 1011–1020. doi:DOI: 10.1016/j.enbuild.2004.06.013.
- [10] J. Heikkinen, Modeling of a supply air terminal for room air flow simulation, in: *Proc. 12th AIVC Conf.*, 1991: pp. 213–230.
- [11] Q. Chen, A. Moser, Simulation of a multiple-nozzle diffuser, in: *Proc. 12th AIVC Conf.*

Ottawa, Canada, 1991: pp. 1–14.

- [12] P. V Nielsen, Computational fluid dynamics and room air movement, *Indoor Air*. 14 (2004) 134–143. doi:10.1111/j.1600-0668.2004.00282.x.
- [13] H. Kotani, K. Sagara, T. Yamanaka, K. Fukumoto, Modelling of Multi-cone Ceiling Diffuser by BOX Method for CFD Analysis of Room Airflow, in: *Roomvent 2007 10th Int. Conf. Air Distrib. Rooms*, 2007.
- [14] R.H. Mohammed, A simplified method for modeling of round and square ceiling diffusers, *Energy Build.* 64 (2013) 473–482. doi:10.1016/j.enbuild.2013.05.021.
- [15] J. Srebric, Q. Chen, Simplified numerical models for complex air supply diffusers, in: *Int. J. Heating, Vent. Air-Conditioning Refrig. Res.*, 2002: pp. 277–294.
- [16] A. Jurelionis, L. Gagytė, T. Prasauskas, D. Čiužas, E. Krugly, L. Šeduikytė, D. Martuzevičius, The impact of the air distribution method in ventilated rooms on the aerosol particle dispersion and removal: The experimental approach, *Energy Build.* 86 (2015) 305–313. doi:10.1016/j.enbuild.2014.10.014.
- [17] J.R. Fontaine, R. Rapp, H. Koskela, R. Niemelä, Evaluation of air diffuser flow modelling methods experiments and computational fluid dynamics simulations, *Build. Environ.* 40 (2005) 377–389. doi:10.1016/j.buildenv.2004.06.021.
- [18] L. Zhou, F. Haghighat, Simplified Method for Modeling Swirl Diffusers, in: *6th Int. Conf. Indoor Air Qual. Vent. Energy Conserv. Build.*, Sendai, Japan, 2007: pp. 333–340.
- [19] Z. Liu, Q. Li, T. Ishihara, Numerical investigation of a swirl diffuser with a novel design using large eddy simulations, *Build. Environ.* 135 (2018) 124–141. doi:10.1016/J.BUILDENV.2018.02.045.
- [20] Y.H. Yau, K.S. Poh, A. Badarudin, A numerical airflow pattern study of a floor swirl diffuser for UFAD system, *Energy Build.* 158 (2018) 525–535. doi:10.1016/J.ENBUILD.2017.10.037.
- [21] M. Jaszczur, M. Borowski, M. Karch, M. Branny, The study of the velocity field of the air flowing the swirl diffusers using PIV method, in: *EPJ Web Conf.*, 2017. doi:10.1051/epjconf/201714302047.
- [22] S.C. Hu, Airflow characteristics in the outlet region of a vortex room air diffuser, *Build. Environ.* 38 (2003) 553–561. doi:DOI: 10.1016/S0360-1323(02)00187-7.
- [23] V. Yakhot, S.A. Orszag, Renormalization group analysis of turbulence. I. Basic theory, *J. Sci. Comput.* 1 (1986) 3–51. doi:10.1007/BF01061452.
- [24] Z.J. Zhai, Z. Zhang, W. Zhang, Q.Y. Chen, Evaluation of Various Turbulence Models in Predicting Airflow and Turbulence in Enclosed Environments by CFD: Part 1—Summary of Prevalent Turbulence Models, *HVAC&R Res.* 13 (2007) 853–870. doi:10.1080/10789669.2007.10391459.
- [25] FLUENT, *Fluent 12.0 user's guide*, Fluent Inc., Lebanon, NH, 2009.
- [26] S. Patankar, *Numerical heat transfer and fluid flow*, CRC press, 1980.
- [27] M.D. Schmidt M, Streblov R, CFD modeling of complex air diffusers, in: *11th Int. Conf. Air Distrib. Rooms, ROOMVENT 2009*, Busan, Korea, 2009.

